Impact of tool-related parameters during fabrication of dissimilar AISI 1010 – CDA 101 joints by FSW

K. Anil Basha [a,*], P. Sevvel [b], K. Giridharan [c]

a. Department of Mechanical Engineering, GRT Institute of Engineering and Technology, Tamil Nadu, India.
b. Department of Mechanical Engineering, S.A.Engineering College (Autonomous), Tamil Nadu, India.
c. Department of Mechanical Engineering, Easwari Engineering College (Autonomous), Tamil Nadu, India.

* Corresponding author: basha301@gmail.com (K. Anil Basha)

Keywords	Abstract
	An experimental endeavor was made to determine suitable tool geometry and ideal values of travel speed, tilt angle, pin offset distance for fabricating 5 mm thick dissimilar AISI 1010 and CDA 101 joints by Friction Stir Welding (FSW). Two differents sets of experiments were performed at constant 1200 rpm employing tools with distinct geometries and varying combinations of tool-related parameters. Reports affirmed the attainment of flawless joints during 2nd set of experimentation by employing a cylindrical shouldered tool (25 mm in diameter) having a cylindrically tapered pin at 1200 rpm, 40 mm/min travel speed, by tilting the tool at $2°$, with its pin being inserted a 1.5 mm offset distance towards CDA 101 plate. Downward axial force of 7.214 kN was found to be ideal for joining these dissimilar metals and it was majorly influenced by the tool's travel speed and pin's offset distance. Presence of different sized Cu particles in AISI matrix, have led to the creation of brittle natured and large intermetallic amalgamations in nugget zone, thereby reducing the strength of fabricated defect-free weldment & leading to a diversified combination of brittle–ductile mode of fracture exhibiting a strength of 181 MPa.

1. Introduction

Steel exhibits admirable weldability and desirable non-hardening features, at low volumes of carbon content. This type of low carbon steels like AISI 1010 grade (having carbon content <0.15%) is widely employed for fabricating flat-rolled commodities including strips, sheets etc., [1,2]. In recent decades, these grades of low carbon steels are now fabricated as Al removed, uninterrupted cast components and supplied to meet a wide range of diversified applications covering home appliances, automotive body cabinets, thin-walled tanks etc., [3–5]. At the same time, their tendency to get corroded easily degrades the lifetime of the components fabricated using this low carbon steels and creates a necessity to join them together with other different metals, especially like copper to increase the corrosion resistance of products [6,7].

Cu (Copper) and its alloy including CDA 101 are familiar or their unique and appealing features with respect to workability and metallurgical characteristics specifically high thermal and electrical conductivity, excellent resistance to corrosion, high ductility [8]. Thermal conductivity of Cu is at most 9–10 times higher than that of various grades of steel [9,10]. There exists a huge demand for products composed of pairs of steel and Cu materials, for various cooling system-based appliances, to prevent unpalatable heating in thermal pipe connections, as electrodes in various machines and equipment concerned with electrical discharging process etc., [11,12].

At the same time, attaining of dissimilar welded joints of Cu and other materials like steel, through fusion based joining techniques is very difficult and resulting joints exhibits undesirable mechanical characteristics, because of the occurrence of intermetallic brittle compound lamina at weld interface [13,14]. Especially, the joints between alloys of Cu and various grades of steels obtained by fusion joining techniques exhibits development of cracks, generation of undesirable intermetallic phases etc., [15–17]. Hence, identification of a suitable technique to weld together alloys of Cu and steel, is essentially necessary.

1.1. Literature survey

Experimental attempts by various researchers have been carried out to join alloys of Cu with various grades of steel by employing several unconventional and solid-state based welding techniques [18–28]. For instance, hybrid laser – cold metal transfer welding was employed to obtain butt joints of 304 stainless steel (SS) & T2 grade Cu, by Meng et al. [19] by straying the beam of laser from the border of the seam of joint to the plate of Cu.

A strategy for obtaining thick SS and CU (3161 & TU1) clad plates by applying explosive welding was established by Wang et al. [20] by combining numerical analysis and real-time experimental runs and the obtained dissimilar clad plates were employed to fabricate high-quality nuclear fusion reactor related devices and equipment. Caligulu et al. [23] made an investigational attempt to join a 12 mm diameter dissimilar AISI 1010 and Cu alloys using the technique of friction welding. Apart from the employment of these various solid-state joining methodologies, an attempt to join dissimilar Cu and AISI 1015 (mild steel) using the induction welding technique was made [26] under the application of different settings of current and loads.

From the above-mentioned detailed literature survey, major drawbacks of these techniques where they are quite costlier, not friendly to the environment, requires high technical and skilled labor etc., [29,30]. As a result, there exists a need for identifying a suitable technique for joining CDA 101 & AISI 1010, which can fabricate sound joints, eliminating the various drawbacks associated with other joining techniques.

1.2. Need for FSW

Friction Stir Welding (FSW) will be an effective joining technique that will overwhelm the various drawbacks of other welding techniques [31,32]. It is a well-known solid state of hot shear technique, which employs a non-exhaustible tool possessing a cylindrical shoulder and unique pin geometry. FSW technique eliminates the various flaws including porosity, solidification-based cracking, distortion etc., [33-36].

Even though, FSW was employed by several investigators to fabricate dissimilar joints of Al–Mg, Al– Cu, Ti–Steel, Al–Ti etc., FSW based experimental attempts for joining Cu- steel metal combination is very scarce and therefore, in this paper, a detailed experimental investigation was performed to demonstrate the competence of FSW technique to fabricate sound dissimilar CDA 101 and AISI 1010 joints and to understand the impact of the design of the tool and its related parameters including tool pin offset distance, tilt angle of the tool, tool speed of travel as well as downward axial force on quality of dissimilar joints.

2. Procedure of experimental investigation

2.1. Investigational material composition and machine set up

5 mm thick flat plates of low carbon steel, i.e., AISI 1010 and copper alloy, i.e., CDA 101 were taken as materials of investigation. Chemical constituents of AISI 1010 alloy and CDA101 plates are described in Table 1.

Joints were fabricated using a distinctly constructed FSW machine as seen in Figure 1, which comprises of arrangements

Table 1. Chemical constituents of parent metals (wt%).

Parent metal	C	Al	W	Mn	P	Ni	Cu	S	Mn	Cr	Balance
AISI 1010	0.051	0.049	0.05	0.22	0.022	0.021	0.023	0.013	0.0132	0.012	Fe

Parent metal	Fe	Zn	Cr	Si	Pb	Ni	Mn	S	Al	Mg	Balance
CDA 101	0.016	0.014	0.01	0.005	0.0049	0.005	0.0009	0.002	0.001	0.0009	Cu

FSW nachine used in this experiment

Figure 1. FSW machine with enlarged views of the control panel, servo control mechanisms and arrangement of base materials in the fixture.

for adjusting the tilt angle of the tool, unique control panel indicating the values of employed parameters, and specifically designed fixture with clamps for positioning the work pieces. Throughout the entire set of experiments, the flat plate of AISI 1010 was positioned on the side of advancement and CDA 101 was stationed on the side of retreating, based on the proven fact that, placing softer materials at the side of retreating enables a smoother flow of the material towards the zone of nugget and will comfortably facilitate the transfer of the softer material towards the side of advancement [37].

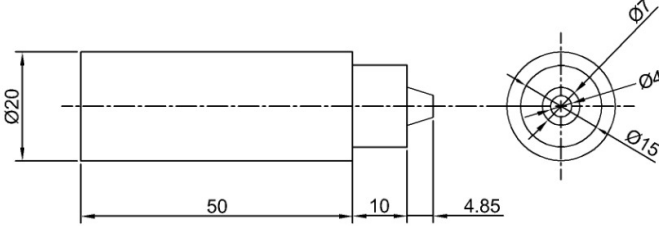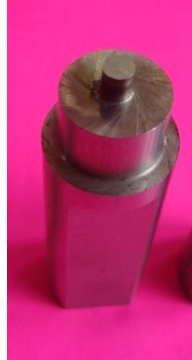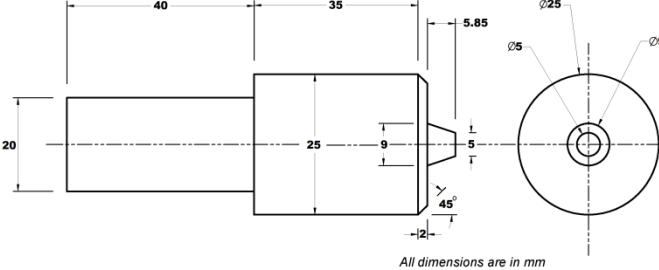### 2.2. Tool design and employed parameters

Experiments were carried out by using 2 tools with different designs specifications and by varying parameters of the FSW technique including tilt angle of the tool, downward axial force, speed of travel of tool, offset distance of tool pin and

with speed of tool rotation etc., remaining constant. Table 2 describes about geometry of 2 tools.

Table 3 provides description of other parameters including tilt angle of the tool, downward axial force, speed of travel, offset distance. Only varying parameter in this experimental set is tool pin offset distance and the varying distances of offset were 1.5 mm, 1.0 mm and 0.5 mm towards the side of CDA 101 plate.

Set 2 experimental set up was framed, based on the observations and results of the joints (J1 to J3) obtained during the first set of the experiments obtained by employing tool design 1. In this set, tool design 2 was employed and was made to travel at four different speeds (i.e., 35, 40, 45 and 50 mm/min) over the joint region at constant rotational speed of 1200 rpm, 2° tilt angle of tool and 1.5 mm offset distance of tool pin, towards CDA 101 plate side.

Table 2. Geometrical specifications of 2 tools.

Tool design	Geometrical design specification	Front view	Tilted top view
Design 1: Cylindrical (straight) pin	ALL DIMENSIONS ARE IN MM		
Design 2: Cylindrical (Taper) pin	All dimensions are in mm		

Table 3. Description of the parameters employed during two experimental sets.

Experimental set no.	Tool design	Joint no.	Tool's speed of rotation	Tool tilt angle	Speed of tool travel	Tool pin offset distance
Set 1	Design 1	J1	1200 rpm	0°	45 mm/min	0.5 mm towards Cu plate
		J2	1200 rpm	1°	45 mm/min	1.0 mm towards Cu plate
		J3	1200 rpm	2°	45 mm/min	1.5 mm towards Cu plate
Set 2	Design 2	J4	1200 rpm	2°	50 mm/min	1.5 mm towards Cu plate
		J5	1200 rpm	2°	45 mm/min	1.5 mm towards Cu plate
		J6	1200 rpm	2°	40 mm/min	1.5 mm towards Cu plate
		J7	1200 rpm	2°	35 mm/min	1.5 mm towards Cu plate

3. Inspection, analysis and perceptions

3.1. Scrutiny of 1st set of joints

Figure 2 reveals photographs of the dissimilar AISI 1010 and CDA 101 joints (J1 to J3) fabricated under 1st set of experimentation. In these images, we can notice the presence of the long continuous cracks on J1 surface, large number of smaller voids on J2 surface and thin void line on J3 surface. The major reason for these categories of visually notable defects is, generation of frictional heat in lower volumes. Lower volumes of heat input occur mainly due to low contact area between surface of tool shoulder and workpiece region. Likewise, high speed of travel of the tool (i.e., high speed of welding), will also generate inadequate heat input, provoking inappropriate mixing of dissimilar materials (i.e., AISI 1010 & CDA 101 in our case), leading to flaws like voids [38].

Macrostructural observations of dissimilar joints (i.e., J1 to J3) fabricated under 1st set of experiments were tabulated in Table 4. Macrostructure of the 1st joint (i.e., J1) clearly shows us, the formation of joint has not at all occurred, which might be resulting from the combined impact of high tool travel speed and 0.5 mm tool offset distance.
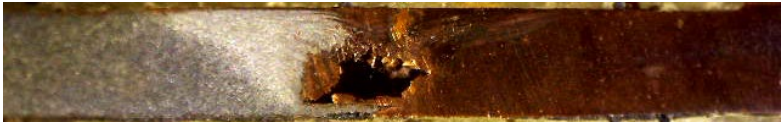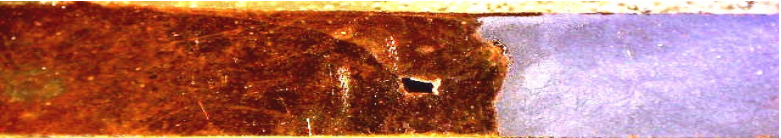
High speed of tool travel had resulted in inadequate metallic bonding and the employed tool offset distance was not sufficient enough to provide uniform flow of the materials from upper to lower and ahead to behind, thereby leading to formation of large sized cavities as seen in J1 macrostructure. Likewise, a large aperture can be seen in the center region of the macrostructure of J2, which extends towards the upper side of the CDA101 and lower region of the AISI 1010 plates. Small tunnel defect was observed in the macrostructure of J3. All these defects help us to understand that, the employed tool shoulder diameter (15 mm) was not large enough to generate sufficient volume of friction heat, as it was a proven fact that, tool shoulder diameter contributes nearly 88% of the heat due to friction, by the action of rubbing of its surface against the surface of the work piece [39,40].

Moreover, these defects also reveal us that, the intermingling of the constituents of AISI 1010 into the matrix of Cu was not consistent from ahead to behind and upper to lower in the nugget of the weld region. This shows us the inefficiency of the geometry of the employed tool pin (i.e., cylindrically straight pin geometry), as the major responsibility of the tool pin is to cleave the material in front and to drive this sheared material behind the tool, thereby stabilizing the joint [41].

Apart from this, the joint (J3) fabricated using $2°$ tool tilt angle was found to possess only a very thin void line, when visually observed.

Table 4. Macro structural observations of dissimilar joints (i.e., J1 to J3) fabricated under the 1st set of experiments.

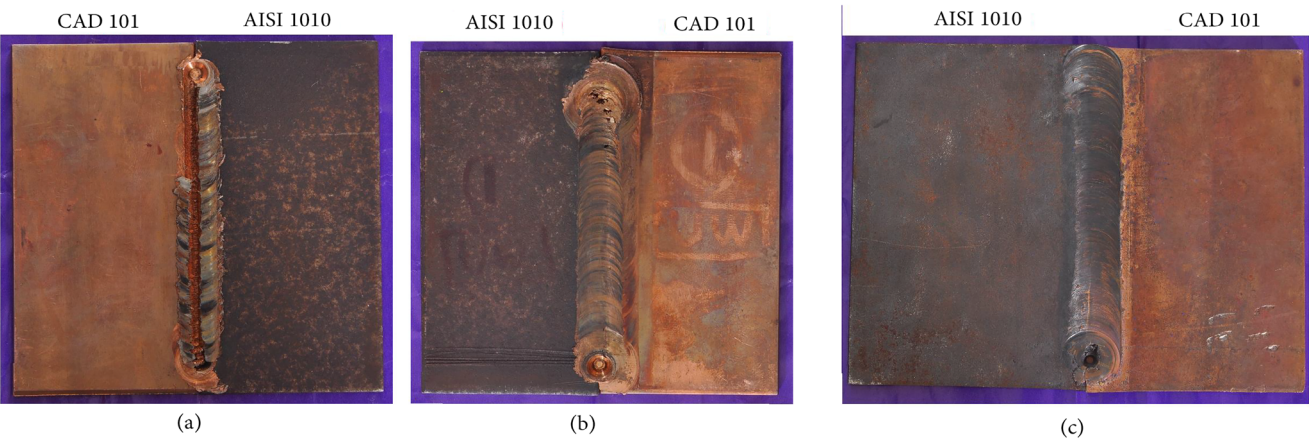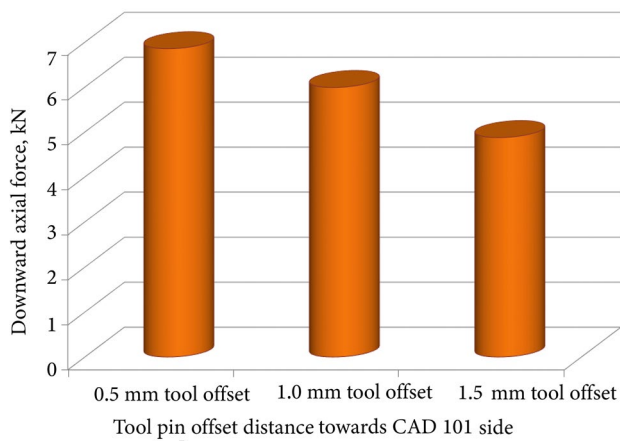| Experimental set no.	Tool design	Joint no.	Macro structure
Set 1	Design 1	J1	
		J2	
		J3	

Figure 2. Dissimilar AISI 1010 and CDA 101 (a) Joint no.: J1 (b) Joint no.: J2 (c) Joint no.: J3 under 1st set of experimentation.

Figure 3. Values of the downward axial force for the various employed tool pin offset distances during the fabrication of the joints (J1, J2 & J3) under the 1st set of experimentation.

This is not in the case of other two joints (J1 and J2), as these joints were having major flaws on their surface, being visible to the normal eyes itself. The reason for the flaw-free appearance of J3 joint was the employment of $2°$ tool tilt angle, as this tilt angle must have ensured the tight holding of the stirred material beneath the tool shoulder and have increased the action of forging, permitting flexible flow of AISI 1010 constituents over the Cu matrix, providing a smooth mixing finish (with negligible visible flaws) on the top surface of the joint, making it most ideal tilt angle when compared with that of the other two angles (i.e., $0°$ and $1°$). Formation of tunnel defect in this joint (J3) would have occurred due to an inappropriate combination of other parameters.

Measurement of the downward axial force using the load cells placed under the specially designed fixture for the various employed tool pin offset distances during the fabrication of the joints (J1, J2 & J3) under the 1st set of experimentation is graphically portrayed in Figure 3.

It can be conceived from these graphs that, the downward axial force decreases with the increase in the tool pin offset distance (i.e., from 0.5 mm to 1.5 mm). Reason for this is that, inserting the tool pin more towards the softer material side (i.e., 1.5 mm towards CDA 101 plate side) ideally disseminates the stresses (thermal nature) to both the metals, thereby generating more heat on the CDA 101 side compared to AISI 1010 side, controlling the fragment formation in the zone of stir and promoting excellent stirring [42]. Due to these facts, less amount of downward axial force would have been needed to rotate the tool pin for performing the stirring action and for blending materials together and as a result, the decrease in the downward axial force have occurred during the fabrication of J3, as shown in Figure 3.

3.2. Selection of parameters for 2nd set of joints

Photographs of the dissimilar AISI 1010 and CDA 101 joints (J1 to J3) fabricated under 1st set of experimentation can be seen in Figure 2. In these images, we can notice the presence of the long continuous cracks on J1 surface, large Inferences made from the examinations of the joints fabricated under 1st set of experimentation strongly suggested that, the diameter of the employed tool has to be increased and the geometry of the tool, i.e, the cylindrically straight pin was

not an ideal design. Based on these inferences, it was decided to increase the shoulder diameter of the tool shoulder from 15 mm to 25 mm. Likewise, instead of a cylindrically straight pin geometry, a tool with cylindrical taper pin geometry was employed for the 2nd set of experimentation, as illustrated in the geometrical design specification of Table 2. Moreover, it was decided to use a constant tool tilt angle of $2°$ and tool offset distance of 2 mm towards the CDA 101 side for the entire set of this experimentation, as the joint (J3) fabricated by this angle permitted flexible flow of AISI 1010 constituents over the Cu matrix, thereby providing a smooth mixing finish (with negligible visible flaws) on the top surface of the joint.

The selection of the values of speed of travel of the tool is an intricate chore, as this parameter has an undeniable impact on the evolution of the intermetallic compounds, creation of distinctive flow stresses and obviously on the joint quality [43]. It was confirmed by several investigations [44,45] during the joining of dissimilar materials by FSW that, the decrease of speed of joining (i.e., speed of travel of tool) at fixed rotational tool speeds and increase of this rotational speed at fixed joining speed exhibits similar material flow (may be desirable or undesirable) during joint fabrication. So, there exists a need for determining the ideal combination of the tool travel speed and its rotational speed with respect to joining of dissimilar metals, especially for joining AISI 1010 and CDA 101 plates and hence it was decided to carry out the 2nd set of experimentation employing four different speeds of tool travel (50, 45, 40 and 35 mm/min) at the constant rotational speed of 1200 rpm.

3.3. Inferences from 2nd set of joints

Photographs of the dissimilar AISI 1010 and CDA 101 joints (J4 to J7) fabricated under 2nd set of experimentation are displayed in Figure 4. The structural morphology of these joints seems to be highly improved when compared with that of the 1st set of joints. Almost all the fabricated joints seem to be free from defects and flaws, when observed visually and to confirm, they are subjected to macro-structural analysis. Macrostructural observations of dissimilar joints (i.e., J4 to J7) fabricated under the 2nd set of experiments were tabulated in Table 5.

From these macrostructural images, we can notice that, the defect intensity was very much high for 1st joint in this set (i.e., J4) in which the speed of tool travel was 50 mm/min and this intensity of defect was found to reduce with the decrease of the speed of the tool speed travel, with other parameters remaining constant. J6 was found to be free from defects entirely, i.e., the joint fabricated at a 40 mm/min tool speed travel. At the same time, when this tool travel speed is further reduced to 35 mm/min, it does not yield a flawless defect, on the contrary, we can notice the occurrence of the defects at the joint's (J7) bottom portion.

The major reason for this decline of defect intensity, followed by defect-free weldment and again occurrence of defects in these fabricated joints is the impact of the travel speed of the tool. It was recorded that, the volume of generated friction heat is conversely proportionate to the speed of welding (i.e., tool's travel speed) [32,46].

Table 5. Macro structural observations of dissimilar joints (i.e., J4 to J7) fabricated under the 2nd set of experiments.
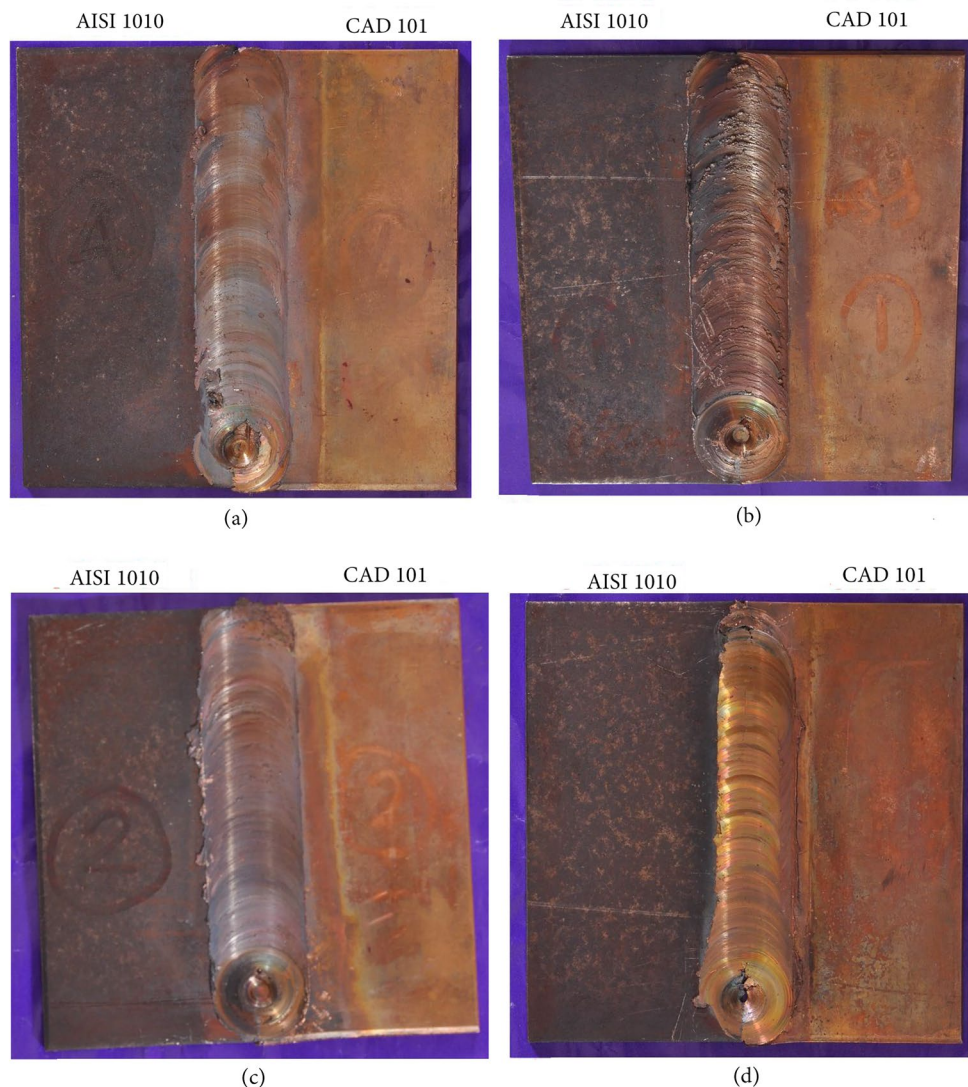
Experimental set no.	Tool design	Joint no.	Macro structure
Set 2	Design 2	J4	
		J5	
		J6	
		J7	

Figure 4. Photographs of dissimilar AISI 1010 and CDA 101 (a) Joint no.: J4 (b) Joint no.: J5 (c) Joint no.: J5 (d) Joint no.: J6 fabricated under 2nd set of experimentation.

For example, in the case of our 1st joint during the 2nd set of experimentation (i.e., J4), travel of tool at higher speed (50 mm/min) have generated lower levels of heat input, contributing to inappropriate mixing of AISI – CDA particles and poor binding of these metallic constituents, which had led to the development of the incomplete joint interfaces as seen in its macrostructure. At the same time, travel of tool at a lower speed (35 mm/min), had resulted in the generation of

higher volumes of frictional heat (normally termed as hot welds) and this surplus frictional heat had initiated larger vertical flow of the softened materials towards the joint center, thereby leading to formation small pores in the lower portion of the fabricated joint (J8). At the same time, the joint fabricated at 45 mm/min (J5) has experienced a minimum level of defects at the lower intersection region of the CDA – AISI constituents.

During this joint fabrication, due to the fact that, decreasing the speed of tool travel (from 50 to 45 mm/min) at a constant speed of tool rotation (1200 rpm), the frictional heat had generated in larger volumes. At the same time, this volume of heat was not sufficient enough to fabricate defect-free dissimilar joints of AISI 1010 – CDA 101 and due to this generated heat, CDA 101 constituents get softened and deformed plastically, followed by their turbulent flow towards the zone of stir. At the same time, this generated heat was not sufficient enough to soften the constituents of AISI 1010 completely and these incompletely softened AISI 1010 constituents have distributed differently in the same zone of stir, which being getting intermingled to completely deformed and softened CDA 101 constituents. This had resulted in the formation of intermetallic compounds in larger numbers in that zone of stir. These intermetallic compounds are very harder and much sensitive to the formation of cracks, will obviously reduce the strength of the joint [31,36].

Joint fabricated at 40 mm/min travel speed was found to be free from defects completely. This must have happened as, further decrease of the speed of tool travel (50 to 40 mm/min) at a constant speed of tool rotation (1200 rpm), must have generated larger volumes of frictional heat, which would have been ideal enough to increase the temperature of the weld zone, thereby reducing the stresses and resulting in the optimal flow of the plasticized material from both the sides and minimizing the occurrence of all sorts of defects, especially cavities, key holes etc., [35] Apart from this welding speed, the tool's rotational speed, its shoulder and pin geometry have also a crucial role in fabricating this defect-free joint.

For instance, employment of still larger rotational speeds (1300, 1400, 1500 rpm etc) would have created a superfluous stirring, leading to detachment of a large number of AISI 1010 particles, too hefty to be dispersed uniformly in the nugget zone, ultimately resulting in inappropriate bonding, followed by voids, cracks etc. Likewise, the adopted pin geometry (i.e., cylindrical taper pin) was ideal enough to perfectly shear the material ahead of it, to provide sufficient stirring action to the softened materials and to move them beneath the tool, thereby consolidating the weldment.

At the same time, the adopted tilt angle of the tool (i.e., 2°) was also appropriate enough and served the function of strongly holding together the stirred constituents under the ideal shoulder diameter (25 mm) combination and enforcing the appropriate transfer of the softened material from upper to lower and from ahead to behind in combination with stirring action of the taper cylindrical pin geometry, resulting in superior bonding between the metallic constituents, providing improved strength to the weldment, which would not have happened during the employment of 0° and 1° tilt angles.

3.4. Analysis of microstructure

To have an understanding about the phenomenon behind the attainment of defect-free weldment, the joint fabricated at 40 mm/min (J6) was observed under an optical microscope and the recorded microstructural images of the various regions of this defect-free weldment are illustrated in Figure 5(a)–(h). One of the parent metal's (CDA 101) microstructure was illustrated in Figure 5(a), which shows the existence of large-sized grains (ranging around 27–31 microns) of Cu together with precipitates of Cu_2O at the boundaries of grain. Another parent metal's (AISI 1010) microstructure was illustrated in Figure 5(h), which shows the appearance of quite larger pearlite grains (ranging around 37–41 microns) embedded in matrixes of ferrite and flow of these grains have occurred during the cold working of AISI 1010 plate, seems to be directed in the forming direction. The micrographs obtained from the heat-affected zone of CDA 101 and AISI 1010 are described in Figure 5(b) and (g) respectively, in which we can observe that, generated frictional heat due to the tool shoulder (25 mm diameter) rotation, have heated up the grains in this region to a larger extent, when compared with that of the grains in the AISI side (because of the adoption of an offset distance of 1.5 mm towards Cu plate).

Recrystallization of Cu grains had started in these regions of CDA 101 plate, leading to slight transformation in the size of the grains. As the grains in the AISI 1010 side have not experienced the full extent of the generated frictional heat, the grains in this region have not transformed completely and there exists the presence of some large-sized pearlite grains here and there in this heat-affected region, as seen in Figure 5(g).

In Figure 5(c), we can witness the combined impacts of pressure exerted by the 2°-tilt angle under a 25 mm tool shoulder surface at a speed of travel of 40 mm/min, which had made the plasticized and softened grain constituents in the thermo-mechanically influenced region of CDA 101, to flow and orient in the direction of the rotation of the stirring taper cylindrical pin. This unique flow of plastically deformed material constituents will happen only at ideal combinations of various parameters of this FSW technique and it is evident, that we have adopted that ideal combination for fabricating this joint [17,33].

This orientation of plasticized material had resulted in the formation of fine-sized recrystallized grains which small-sized fragments of AISI constituents in the nugget zone nearer to the CDA 101 side, as seen in Figure 5(d). The size of the Cu grains in this region had also been found to be reduced significantly, thereby contributing to the improved strength of the joint. Likewise, in Figure 5(f), we can observe that the pearlite grains of AISI 1010 have experienced disintegration and underwent a reduction in their size, as seen in the nugget zone nearer to the side of AISI 1010. The junction of the interface of the zone of the nugget is illustrated in Figure 5(e), where we can visualize the fusion of the ingredients of CDA 101 and AISI 1010 perfectly.
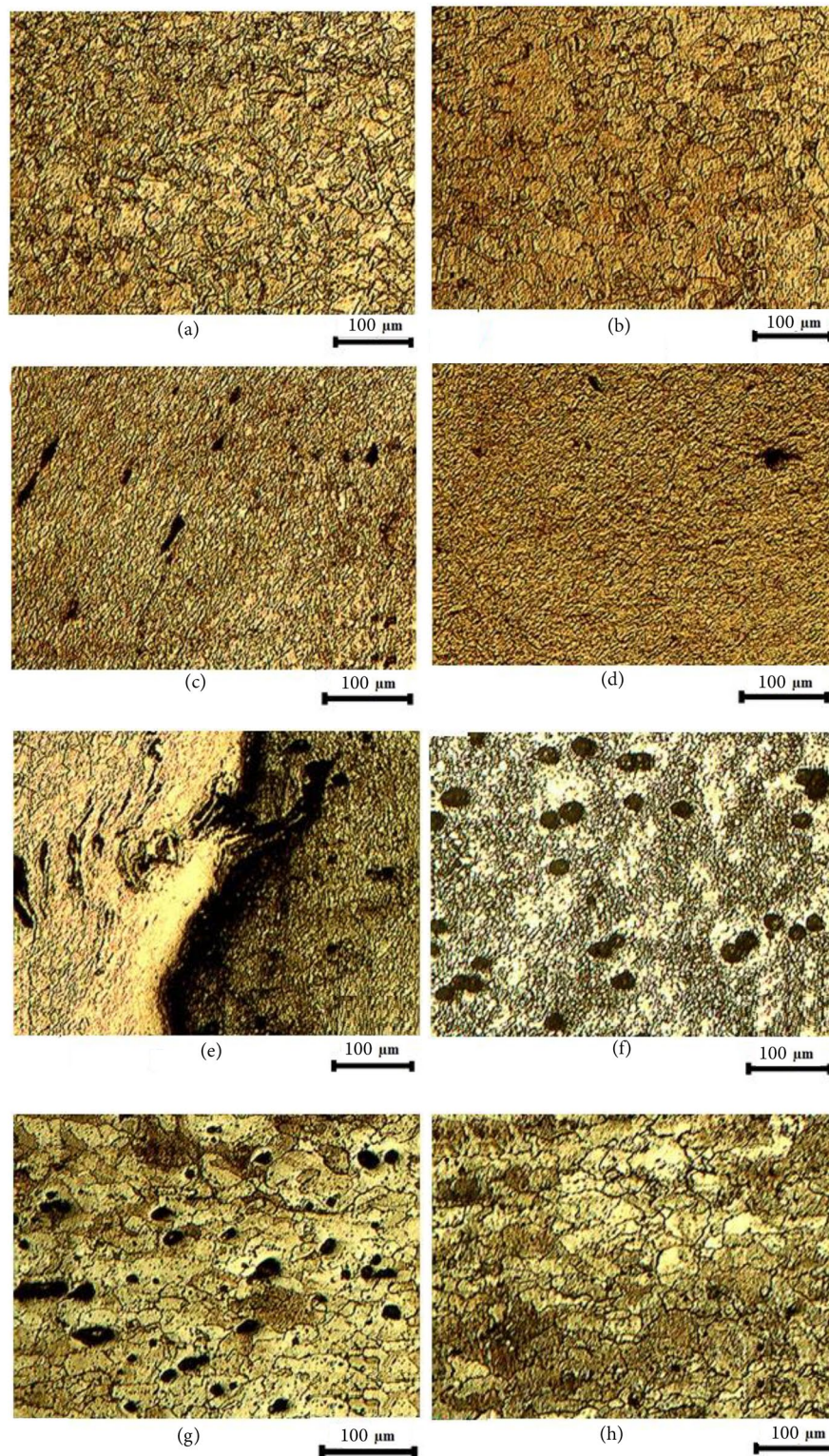
Figure 5. Optical microstructural images of (a) CDA 101 parent metal, (b) CDA101 side's heat-affected zone, (c) CDA101 side's thermo-mechanically affected zone, (d) zone of stir towards CDA101 side, (e) Interfacing junction at zone of stir, (f) zone of stir towards AISI 1010 side, (g) AISI 1010 side's heat-affected zone, and (h) AISI 1010 parent metal fabricated at 40 mm/min (J6).
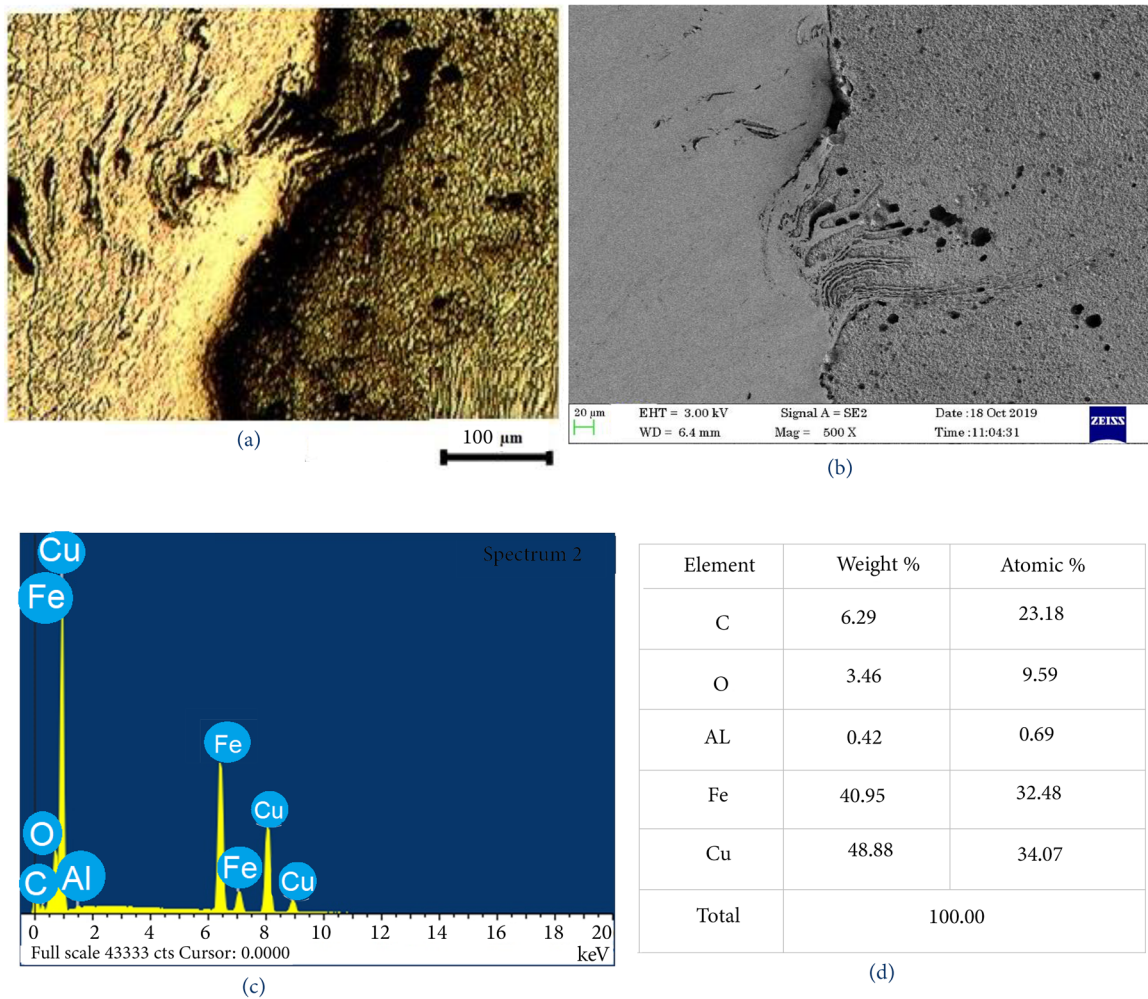
On the left side is the copper and the right side is the steel. Due to the adoption of suitable type of pin geometry (i.e., cylindrical taper pin), its stirring action in perfect combination with the tilt angle (2°), 1200 rpm rotation and 40 mm/min travel speed had softened the materials of CDA 101 and AISI 1010, enabling the mixing of the Cu constituents into the ferrite matrix from ahead to behind and from upper to lower, thereby resulting in improved bonding level between these dissimilar materials. At the same time,

the line of fusion was found to be enriched with constituents of copper and the grains on the side of copper have experienced severe plasticity when compared with that of the grains on the side of the steel, which might be resulting due to the adoption of 1.5 mm offset towards CDA 101 side.

3.5. SEM and EDX images

To justify the above-mentioned fusion of the ingredients of CDA 101 and AISI 1010 in the interface junction, this region

| Element	Weight %	Atomic %
C	6.29	23.18
O	3.46	9.59
AL	0.42	0.69
Fe	40.95	32.48
Cu	48.88	34.07
Total	100.00	

Figure 6. (a) Optical microscopy, (b) SEM image of the interface junction of the dissimilar joint of CDA 101 and AISI 1010 at 40 mm/min (J6) (c) constituents being identified in interface junction by EDX test, and (d) constituents corresponding numerical values of weight and atomic percentages

was subjected to SEM and EDX analysis and Figure 6(a)-(c) illustrates the Scanning Electron Microscopy (SEM) image of this zone, a graphical description of constituents being identified and their numerical values of weight and percentage respectively.

EDX test results that, above mentioned interface region is found to possess 6.29% of carbon, 3.46% of oxygen, 0.42% of aluminium, 40.95% of iron and 48.88% of copper by weight. Occurrences of oxidation amidst the matrixes of steel and copper have been confirmed by the presence of oxygen. The above-mentioned percentages of copper and iron confirm us that, the intermingling of cu constituents into the ferrite matrix from ahead to behind and from upper to lower had occurred. At the same time, this zone was found to be present with more percentage of Cu constituents (48.88%) when compared with the percentage of steel (40.95%), revealing the impact of the adopted 1.5 mm tool offset towards CDA 101 plate.

### 3.6. Determination of downward axial force

Measurement of the downward axial force using the load cells placed under the specially designed fixture for the joints (J4, J5, J6 and J7) under 2nd set of experimentation is graphically portrayed in Figure 7. It can be conceived from these graphs that, the downward axial force decreases with the reduction in the speed of tool travel (i.e., from 50 mm/min
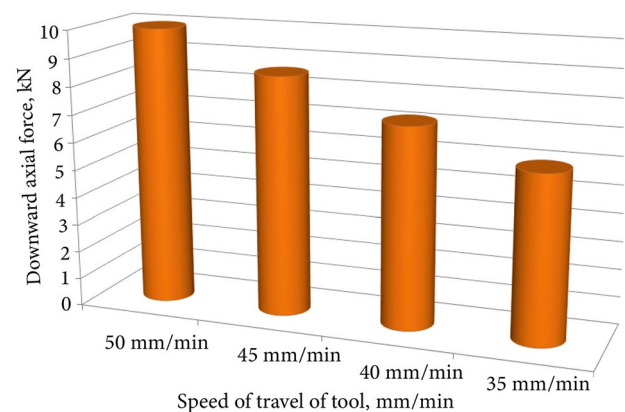
Figure 7. Values of the downward axial force for the joints (J4, J5, J6 and J7) fabricated under the 2nd set of experimentation.

to 35 mm/min). This is due to the reported fact that, at higher joining speeds, less volume of friction heat is generated, as the generation of heat is inversely proportional to the speed of joining. Hence, at lower volumes of heat input (for example during fabrication of J4 at 50 mm/min), the employed tool demands for large amount of downward force axially to perform the stirring action (9.982 kN, as in case of J4) [16,47].

As the speed of tool travel decreases from 50 to 45 mm/min, 40 mm/min and 35 mm/min, there would have been
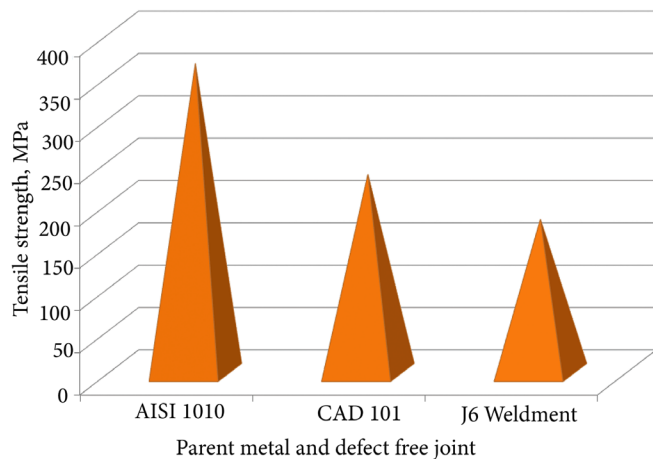
Figure 8. Graphical comparison of the tensile strength of the parent metals (AISI 1010, CDA 101) and defect-free weldment (J6).

an increase in the volume of generated frictional heat, decreasing the quantum of required downward axial force (i.e., 8.589 kN, 7.204 kN and 5.898 kN respectively). From these graphs, we can understand that, the plasticized materials will get flashed out under the higher amount of downward axial force (8.5–10 kN), resulting in defective joints, as observed during the fabrication of J4 and J5 dissimilar AISI 1010 – CDA 101 joints.

At the same time, the lower amount of downward axial force (less than 6 kN) will also result in defective weldment (J7), as this less amount of force will not be sufficient enough to support the vertical circulation of the softened materials. Downward axial force of 7.214 kN was found to be an ideal amount of force for joining dissimilar 3 mm thick flat plates of AISI 1010 and CDA 101, as a defect-free joint was fabricated under this axial force in combination with $2°$ tilt angle, 40 mm/min speed of weld, 1.5 mm tool offset towards Cu side, 1200 speed of rotation, during the employment of a 25mm tool shoulder possessing a cylindrical taper pin.

3.7. Tensile test announcements

To determine the efficiency of the fabricated joint, tensile tests for the parent metals (namely AISI 1010 and CDA 101) and defect-free weldment (J6) were carried out and graphically illustrated in Figure 8.

Defect-free weldment (J6) exhibited a tensile strength of 181 MPa, which is nearly 77% of one of the base materials, namely CDA 101, along with a percentage of elongation of 14.01% and this tensile strength can be considered as an appreciable strength, especially with respect to dissimilar joints [16, 31, 48]. The tensile fractured specimen was subjected to SEM observations, to understand the theory behind this lesser efficiency of joint.

SEM photographs of that defect-free specimen (J6) are exhibited in Figure 9(a)–(e), in which we can entirely zone of fracture with Cu in its top portion and matrix of steel forming the bottom layer. Flat surfaces seen on the Cu side together with fine sized grains revealing the occurrence of superior levels of plasticity, helps us to understand that, these have experienced brittle mode of fracture. At the same time, the presence of small dimples, pores etc., at the bottom portion indicates a ductile mode of failure had occurred in

those portions. Yet, the regions possessing flat regions (which have contributed for ductile fracture) were found to cover more portions of this fracture specimen, when compared to that of those minute dimple structures, which concedes that, this defect-free specimen has experienced a diversified combination of brittle-ductile mode of fracture [18,31].

Apart from this, the major reasons due to which this defect-free joint was unable to exhibit 100% of the tensile strength of the base materials can be understood by closely observing the microstructural image of the nugget zone of this joint illustrated in Figure 5(f). This zone also reveals the presence of Cu particles along with their dispersions. The reason for the penetration of these Cu particles into the AISI matrix, is the stirring action of tool pin, which have pushed these materials beneath it, making them to infiltrate the matrix of AISI 1010. These randomly distributed constituents of Cu found in the matrix of steel, can be mentioned as different shaped islands of Cu in the ocean of Steel matrix. The presence of these different sized Cu particles in AISI matrix, have led to the formation of brittle natured and large intermetallic amalgamations in the nugget zone [49].

The presence of these brittle natured intermetallic compounds had contributed for supplementary brittleness in the zone of stir, thereby reducing the strength and elongation percentage of the fabricated defect-free weldment, due to which attainment of the strengths equivalent to at least one of the parent materials had become impossible [50]. At the same time, this exhibited tensile strength of 181 MPa, which is nearly 77% of one of the base materials, namely CDA 101, along with a percentage of elongation of 14.01% can be considered as an appreciable strength, especially with respect to dissimilar joints [38,51].

4. Conclusions

To understand the impact of the tool geometry and other process variables including tool tilt angle, tool pin offset distance, tool speed travel, during the joining of dissimilar 5mm thick CDA 101 and AISI 1010 flat plates, 2 sets of experiments were carried out by employing two tools with distinctive geometries at constant tool speed rotation of 1200 rpm, by combining different values of other parameters and following inferences were recorded:

- Tool with a 15 mm diameter cylindrical shoulder and cylindrically straight pin geometry was not large enough to generate sufficient volume of friction heat leading to defective joints and inappropriate intermingling of constituents of AISI 1010 into the matrix of Cu revealed the inefficiency of the geometry of that tool pin;

- Defect-free dissimilar joint of AISI 1010 and CDA 101 was attained during the 2nd set of experimentation by employing a cylindrical shouldered tool (25 mm in diameter) along with a cylindrically tapered pin geometry at a speed of rotation of 1200 rpm, 40 mm/min tool travel speed, by tilting the tool at an angle of $2°$, with its pin being inserted a 1.5 mm offset distance of towards the CDA 101 plate;
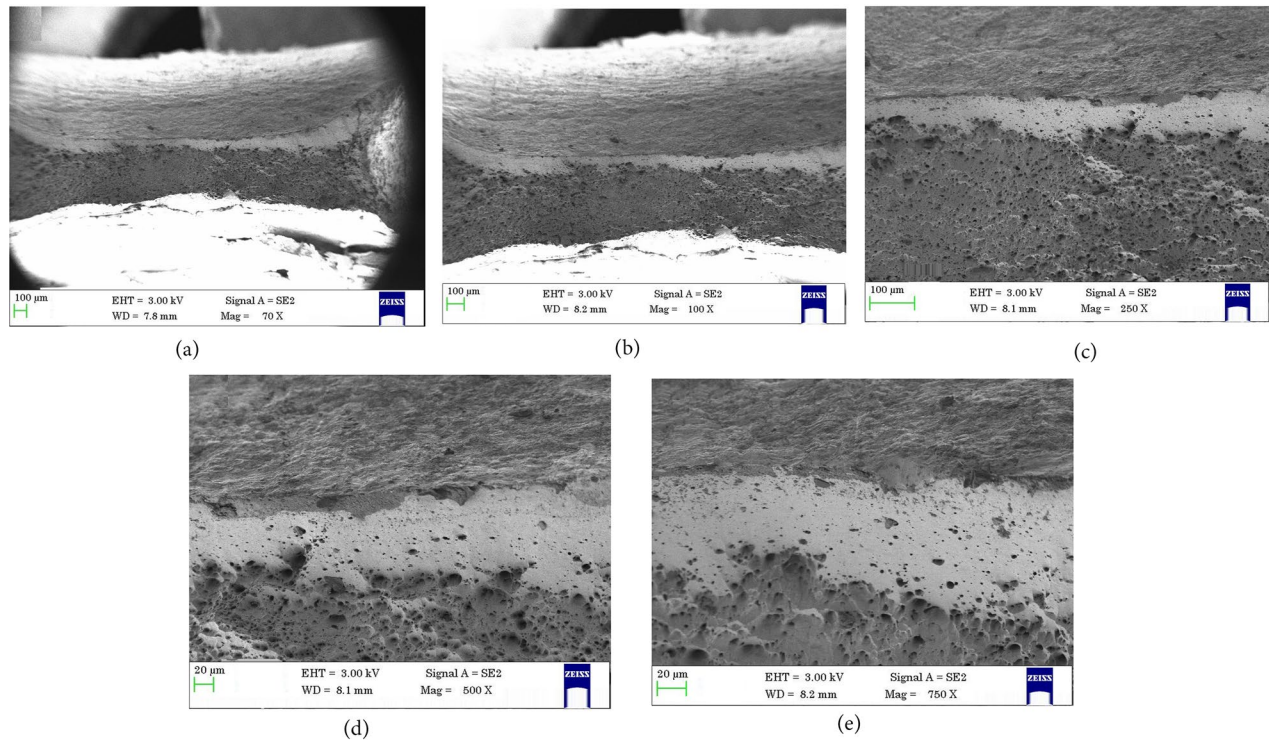
Figure 9. SEM photographs of the fractured tensile specimen on joint fabricated during 2nd set of experimentation at 40 mm/min (J6) at (a) 70× magnification, (b) 100× magnification, (c) 250× magnification, (d) 500× magnification, and (e) 750× magnification.

- It was observed that, the plasticized materials will get flashed out under higher downward axial force (8.5-10 kN), resulting in defective joints and lower downward axial force (less than 6 kN) will also result in defective weldment, as this force will not be enough to support the vertical circulation of the softened materials;
- The downward axial force of 7.214 kN was found to be an ideal amount of force for joining dissimilar 3 mm thick flat plates of AISI 1010 and CDA 101;
- Defect-free weldment (J6) exhibited a tensile strength of 181 MPa, which is nearly 77% of one of the base materials, namely CDA 101, along with a percentage of elongation of 14.01%;
- Diversified combination of brittle–ductile mode of fracture was exhibited by fractured defect-free joint specimen and the presence of different sized Cu particles in AISI matrix, have led to the formation of brittle natured and large intermetallic amalgamations in the nugget zone. These brittle natured intermetallic compounds had contributed to supplementary brittleness, thereby reducing the strength of fabricated defect-free weldment.

Funding

Conflicts of interest

The authors declare that they have no known competing financial interests or personal relationships that could have appeared to influence the work reported in this paper.

Authors contribution statement

First author
Anil Basha K.: Methodology; Investigation; Resources; Writing-original draft preparation.

Second author
Sevvel P.: Conceptualization; Writing-review and editing; Validation; Supervision; Project administration.

Third author
Giridharan K.: Software; Data curation; Visualization; Formal analysis.

References

1. Inose, K., Kanbayashi, J., Abe, D., et al. "Design and welding method for high-strength steel structure using laser-arc hybrid welding", *Welding in the World*, **57**, pp. 657–664 (2013).
https://doi.org/10.1007/s40194-013-0064-0.

2. Yaknesh, S., Sampathkumar, K., Sevvel, P., et al. "Generation of force and torque during joining of AZ91C plates by FSW under distinctive tool tilt angle and their impact on mechanical strength and microstructure", *Journal of Adhesion Science and Technology*, **37**(6), pp. 1071– 1090 (2022).
https://doi.org/10.1080/01694243.2022.2057763.

3. Qi, X., Di, H., Sun, Q., et al. "A comparative analysis on microstructure and fracture mechanism of X100 pipeline steel CGHAZ between laser welding and arc

welding", *Journal of Materials Engineering and Performance*, **28**, pp. 7006–7015 (2019). https://doi.org/10.1007/s11665-019-04412-5.

4. Chen, L., Zhou, L., Tang, C., et al. "Study of laser butt welding of SUS301L stainless steel and welding joint analysis", *The International Journal of Advanced Manufacturing Technology*, **73**, pp. 1695–1704 (2014). https://doi.org/10.1007/s00170-014-5928-y

5. Hassel, T., Konya, R., Collmann, M., et al. "Economical joining of tubular steel towers for wind turbines employing non-vacuum electron beam welding for high-strength steels in comparison with submerged arc welding", *Welding in the World*, **57**, pp. 551–559 (2013). https://doi.org/10.1007/s40194-013-0050-6

6. Shi, Cg., Wang, Y., Li, Sj., et al. "Application and experiment on the least-action principle of explosive welding of stainless steel/steel", *Journal of Iron and Steel Research International*, **21**, pp. 625–629 (2014). http://dx.doi.org/10.1016/S1006-706X(14)60097-2

7. Shmorgun, V.G., Slautin, O.V., and Kulevich, V.P. "Features of diffusion interaction in steel-aluminum composite after explosive welding and aluminizing by melt immersion", *Metallurgist*, **63**, pp. 766–774 (2019). https://doi.org/10.1007/s11015-019-00887-8.

8. Zimniak, Z. and Radkiewicz, G. "The electroplastic effect in the cold-drawing of copper wires for the automotive industry", *Archives of Civil and Mechanical Engineering*, **8**, pp. 173–179 (2008). https://doi.org/10.1016/S1644-9665(12)60204-0

9. Shabani, M.O. and Mazahery, A. "Automotive copper and magnesium containing cast aluminium alloys: Report on the correlation between Yttrium modified microstructure and mechanical properties", *Russian Journal* of *Non-Ferrous Metals*, **55**, pp. 436–442 (2014). https://doi.org/10.3103/S1067821214050150

10. Mehta, K.P. and Badheka, V.J. "A review on dissimilar friction stir welding of copper to aluminum: process, properties, and variants", *Materials and Manufacturing Processes*, **31**(3), pp. 233−254 (2016). https://doi.org/10.1080/10426914.2015.1025971

11. Singh, G., Saxena, R.K., and Pandey, S. "Investigating the effect of arc offsetting in AISI 304 stainless steel and copper welding using gas tungsten arc welding", *Journal of the Brazilian Society of Mechanical Sciences and Engineering*, **43**, p. 174 (2021). https://doi.org/10.1007/s40430-021-02877-x

12. Srinivasan, D. and Ananth, K. "Recent advances in alloy development for metal additive manufacturing in gas turbine/aerospace applications: A review", *Journal of the Indian Institute* of *Science,* **102**, pp. 311–349 (2022). https://doi.org/10.1007/s41745-022-00290-4

13. Chen, S., Huang, J., Xia, J., et al. "Microstructural characteristics of a stainless steel/copper dissimilar joint made by laser welding", *Metallurgical and Materials,* Transactions A, **44**, pp. 3690–3696 (2013). https://doi.org/10.1007/s11661-013-1693-z

14. Asai, S., Ogawa, T., Ishizaki, Y., et al. "Application of plasma MIG hybrid welding to dissimilar joints between copper and steel", *Welding in the World*, **56**, pp. 37–42 (2012). https://doi.org/10.1007/BF03321143

15. Zhang, M., Zhang, Y., Li, J., et al. "Microstructure and mechanical properties of the joint fabricated between stainless steel and copper using gas metal arc welding", *Transactions of the Indian Institute of Metals*, **74**, 969–978 (2021).https://doi.org/10.1007/s12666-021-02208-7

16. Tatarnikov, P.A. and Kharlamov, V.I. "Application of immersive copper coatings with high adhesive strength to steel welding wire", *Steel in Translation*, **41**, pp. 1029–1032 (2011). https://doi.org/10.3103/S0967091211120151

17. Wang, Y., Luo, J., Wang, X., et al. "Interfacial characterization of T3 copper/35CrMnSi steel dissimilar metal joints by inertia radial friction welding", *The International Journal of Advanced Manufacturing Technology*, **68**, pp. 1479–1490 (2013). https://doi.org/10.1007/s00170-013-4936-7

18. Besler, F.A., Grant, R.J., Schindele, P., et al. "Advanced process possibilities in friction crush welding of aluminum, steel, and copper by using an additional wire", *Metallurgical and Materials Transactions B*, **48**, pp. 2930–2948 (2017). https://doi.org/10.1007/s11663-017-1108-4

19. Meng, Y., Li, X., Gao, M., et al. "Microstructures and mechanical properties of laser-arc hybrid welded dissimilar pure copper to stainless steel", *Optics and Laser Technology*, **111**, pp. 140–145 (2019). https://doi.org/10.1016/j.optlastec.2018.09.050

20. Wang, Y., Li, X., Wang, X., et al. "Fabrication of a thick copper-stainless steel-clad plate for nuclear fusion equipment by explosive welding", *Fusion Engineering and Design*, **137**, pp. 91–96 (2018). https://doi.org/10.1016/j.fusengdes.2018.08.017

21. Guo, S., Zhou, Q., Kong, J., et al. "Effect of beam offset on the characteristics of copper/304stainless steel electron beam welding", *Vacuum*, **128**, pp. 205–212 (2016). https://doi.org/10.1016/j.vacuum.2016.03.034

22. Chang, C.C., Wu, L.H., Shueh, C., et al. "Evaluation of microstructure and mechanical properties of dissimilar welding of copper alloy and stainless steel", *The International Journal of Advanced Manufacturing Technology*, **91**, pp. 2217–2224 (2017). https://doi.org/10.1007/s00170-016-9956-7

23. Caligulu, U., Acik, M., Balalan, Z., et al. "The effects of process parameters for joining of AISI 1010-Cu alloys by friction welded", *International Journal of Steel Structures*, **15**, pp. 923–931 (2015). https://doi.org/10.1007/s13296-015-1213-7

24. Mitelea, I., Groza, C., and Craciunescu, C. "Copper interlayer contribution on Nd:YAG laser welding of dissimilar Ti-6Al-4V alloy with X5CrNi18-10 steel", *Journal of Materials Engineering and Performance*, **22**, pp. 2219–2223 (2013). https://doi.org/10.1007/s11665-013-0507-1

25. Koley, S., Akhtar, M.T., Kumar, N., et al. "Effect of secondary coating on weldability, joint performance, and electrode life in resistance seam welding of galvannealed interstitial free steel", *Journal of Materials Engineering and Performance*, **31**, pp. 2432–2444 (2022). https://doi.org/10.1007/s11665-021-06367-y

26. Chen, S., Huang, J., Xia J., Zhang H., et al. "Microstructural characteristics of a stainless steel/copper joint made by laser welding", *Metallurgical and Materials,* Transactions A, **44**(A), pp. 3690–3696 (2013). https://doi.org/10.1007/s11661-013-1693-z

27. Bhogendro Meitei, R.K., Maji, P. Samadhiya, A., et al. "A study on induction welding of mild steel and copper with flux under applied load condition", *Journal of Manufacturing Processes*, **34**(A), pp. 435–441 (2018). https://doi.org/10.1016/j.jmapro.2018.06.029

28. Gladkovsky, S.V., Kuteneva, S.V., and Sergeev, S.N. "Microstructure and mechanical properties of sandwich copper/steel composites produced by explosive welding", *Materials Characterization*, **154**, pp. 294–303 (2019). https://doi.org/10.1016/j.matchar.2019.06.008

29. Bhogendro Meitei, R.K., Maji, P., Samadhiya, A., et al. "An experimental investigation on joining of copper and stainless steel by induction welding technique", *International Journal of Precision Engineering and Manufacturing*, **21**, pp. 613–621 (2020). https://doi.org/10.1007/s12541-019-00284-w

30. Najafi, S., Khanzadeh, M.R., Bakhtiari, H., et al. "Electrochemical investigation of dissimilar joint of pure Cu to AISI 410 martensitic stainless steel fabricated by explosive welding", *Surface Engineering* and *Applied Electrochemistry,* **56**, pp. 675–683 (2020). https://doi.org/10.3103/S1068375520060113

31. Tiwari, A. Pankaj, P., Biswas, P., et al. "Tool performance evaluation of friction stir welded Shipbuilding grade DH36 steel butt joints", *The International Journal of Advanced Manufacturing Technology*, **103**, pp. 1989–2005 (2019). https://doi.org/10.1007/s00170-019-03618-0

32. Akbari, M. and Asiabaraki, H.R. "Modeling and optimization of tool parameters in friction stir lap joining of aluminum using RSM and NSGA II", *Welding International*, **37**(1), pp. 21–33 (2023). https://doi.org/10.1080/09507116.2022.2164530

33. Steuwer, A., Barnes, S.J., Altenkirch, J., et al. "Friction stir welding of HSLA-65 steel: Part II. The influence of weld speed and tool material on the residual stress distribution and tool wear", *Metallurgical and Materials,* Transactions A, **43**(7), pp. 2356–2365 (2012). https://doi.org/10.1007/s11661-011-0643-x

34. Dhanesh Babu, S.D., Sevvel, P., Senthil Kumar, R., et al. "Development of thermo mechanical model for prediction of temperature diffusion in different FSW tool pin geometries during joining of AZ80A Mg alloys", *Journal of Inorganic and Organometallic Polymers and Materials*, **31**(7), pp. 3196–3212 (2021). https://doi.org/10.1007/s10904-021-01931-4

35. Singh, S.H. and Mahmeen M. "Effect of tool pin offset on the mechanical properties of dissimilar materials based on friction stir welding (FSW)", *International Journal of Modern Trends in Engineering and Research*, **3**, 75−80 (2016).

36. Thomae, M., Gester, A., and Wagner, G. "Comparison of process behavior, microstructure and mechanical properties of ultrasound enhanced friction stir welded titanium/titanium joints", *Welding in the World*, **66**, pp. 1131–1140 (2022). https://doi.org/10.1007/s40194-022-01279-4

37. Akbari, M., Aliha, M.R.M., and Berto, F. "Investigating the role of different components of friction stir welding tools on the generated heat and strain", *Forces in Mechanics*, **10**, 100166 (2023). https://doi.org/10.1016/j.finmec.2023.100166

38. Giridharan, K., Sevvel, P., Ramadoss, R., et al. "Friction stir processing of nanofiller assisted AISI 1010 steel-CDA 101 copper dissimilar welds: a strength factor approach", *Metallurgical Research and Technology*, **119**, p. 505 (2022). https://doi.org/10.1051/metal/2022065

39. Sarikavak, Y. "An advanced modelling to improve the prediction of thermal distribution in friction stir welding (FSW) for difficult to weld materials", *Journal of the Brazilian Society of Mechanical Sciences and Engineering*, **43**, p. 4 (2021). https://doi.org/10.1007/s40430-020-02735-2

40. Esmaeili, A., Besharati G.M., and Zareie R.H. "Experimental investigation of material flow and welding defects in friction stir welding of aluminum to brass", *Materials and Manufacturing Processes*, **27**(12), pp. 1402−1408 (2012). http://dx.doi.org/10.1080/10426914.2012.663239

41. Abdollah-Zadeh A., Saeid T., and Sazgari B. "Microstructural and mechanical properties of friction stir welded aluminum/copper lap joints", *Journal of Alloys and Compounds*, **460**(1), pp. 535−538 (2008). https://doi.org/10.1016/j.jallcom.2007.06.009

42. Galvao, I., Leal, R., Loureiro, A., et al. "Material flow in heterogeneous friction stir welding of aluminium and copper thin sheets", *Science and Technology of Welding and Joining*, **15**(8), pp. 654−660 (2010). http://dx.doi.org/10.1179/136217110X12785889550109

43. Rai, R., De, A., Bhadeshia, H., et al. "Review: Friction stir welding tools", *Science and Technology of Welding and Joining*, **16**(4), pp. 325−342 (2011). http://dx.doi.org/10.1179/1362171811Y.0000000023

44. Patil, H. and Soman, S. "Experimental study on the effect of welding speed and tool pin profiles on AA6082-O aluminium friction stir welded butt joints", *International Journal of Engineering, Science and Technology*, **2**(5), pp. 268−275 (2010). https://doi.org/10.4314/ijest.v2i5.60163

45. Liu, F.C., Hovanski, Y., Miles, M.P., et al. "A review of friction stir welding of steels: Tool, material flow, microstructure, and properties", *Journal of Materials Science and Technology*, **34**(1), pp. 39−57 (2018). https://doi.org/10.1016/j.jmst.2017.10.024

46. Abbasi, M., Abdollahzadeh, A., Bagheri, B., et al. "The effect of SiC particle addition during FSW on microstructure and mechanical properties of AZ31 magnesium alloy", *Journal of Materials Engineering and Performance*, **24**, pp. 5037–5045 (2015). https://doi.org/10.1007/s11665-015-1786-5

47. Joshi, G.R. and Badheka, V.J. "Microstructures and properties of copper to stainless steel joints by hybrid FSW", *Metallography, Microstructure, and Analysis*, **6**, pp. 470–480 (2017). https://doi.org/10.1007/s13632-017-0398-x

48. Gotawala, N. and Shrivastava, A. "Thermodynamics-based analysis of formation and growth of FeTi and β-Ti during friction stir welding of SS304 and pure titanium", *Journal of Materials Science*, **56**, pp. 19180–19198 (2021). https://doi.org/10.1007/s10853-021-06491-z

49. Asadi, P., Mirzaei, M.H., and Akbari, M. "Modeling of pin shape effects in bobbin tool FSW", *International Journal of Lightweight Materials and Manufacture*, **5**(2), pp. 162–177 (2022). https://doi.org/10.1016/j.ijlmm.2021.12.001

50. Akbari, M., Ezzati, M., and Asadi, P. "Investigation of the effect of tool probe profile on reinforced particles distribution using experimental and CEL approaches", *International Journal of Lightweight Materials and Manufacture*, **5(2)**, pp. 213–223 (2022). https://doi.org/10.1016/j.ijlmm.2022.02.002

51. Tiwari, A., Singh, P., and Pankaj, P., et al. "FSW of low carbon steel using tungsten carbide (WC-10wt.%Co) based tool material", *Journal* of *Mechanical Science* and *Technology*, **33**, pp. 4931–4938 (2019). https://doi.org/10.1007/s12206-019-0932-7

Biographies

K. Anil Basha is currently pursuing his Doctoral degree (PhD) in Mechanical Engineering, Anna University, Chennai, India. He has more than 8 years of teaching experience. He is currently serving as Assistant Professor, Department of Mechanical Engineering in GRT Institute of Engineering and Technology, Tiruvallur District, Tamil Nadu, India. He has published several research papers in the area of Friction Stir Welding in renowned international journals indexed in Scopus.

P. Sevvel obtained his PhD in Mechanical Engineering from Anna University, Chennai in 2016 and successfully completed his Masters of Technology. degree with 1st Class Distinction in Industrial Engineering from the National Institute of Technology (NIT) Trichy, India, in 2005. He has a total of more than 17 years of teaching experience. He is currently working as Professor, Department of Mechanical Engineering College in S.A. Engineering College (Autonomous), Chennai. He has published more than 46 Research Papers in various SCI and Scopus indexed international journals. He is currently guiding a total of 9 research scholars pursuing their PhD in center for research, Anna University. He was awarded with BEST RESEARCHER AWARD for his distinct contribution in the field of Materials Science during the 6th Annual Millennium Impact Award 2020.

K. Giridharan obtained his PhD in Mechanical Engineering from Anna University, Chennai in the year 2022. He has a total of more than 10 years of teaching experience. He is currently working as Assistant Professor, Department of Mechanical Engineering College in Easwari Engineering College (Autonomous), Chennai, Tamil Nadu, India. He has published several research papers in various SCI and Scopus indexed international journals.